Artificial neural network model for material characterization by indentation

2004 Modelling Simul. Mater. Sci. Eng. 12 1055

(http://iopscience.iop.org/0965-0393/12/5/019)

INSTITUTE OF PHYSICS PUBLISHING MODELLING AND SIMULATION IN MATERIALS SCIENCE AND ENGINEERING

Modelling Simul. Mater. Sci. Eng. **12** (2004) 1055–1062 PII: S0965-0393(04)80088-3

Artificial neural network model for material characterization by indentation

K K Tho[1], S Swaddiwudhipong[1], Z S Liu[2] and J Hua[1]

[1] Department of Civil Engineering, National University of Singapore, 119260 Singapore
[2] Institute of High Performance Computing, 1 Science Park Road, #01-01, 117528 Singapore

Received 19 April 2004
Published 12 August 2004
Online at stacks.iop.org/MSMSE/12/1055
doi:10.1088/0965-0393/12/5/019

Abstract

Analytical methods to interpret the indentation load–displacement curves are difficult to formulate and solve due to material and geometric nonlinearities as well as complex contact interactions. In this study, large strain–large deformation finite element analyses were carried out to simulate indentation experiments. An artificial neural network model was constructed for the interpretation of indentation load–displacement curves. The data from finite element analyses were used to train and validate the artificial neural network model. The artificial neural network model was able to accurately determine the material properties when presented with the load–displacement curves that were not used in the training process. The proposed artificial neural network model is robust and directly relates the characteristics of the indentation load–displacement curve to the elasto-plastic material properties.

1. Introduction

Materials characterization can be carried out based on the results obtained from instrumented indentation tests. Besides the hardness of materials, recent research efforts have focused on the interpretation of indentation load–displacement curves for other basic mechanical material properties, such as Young's modulus, yield strength and strain-hardening exponent. Doerner and Nix [1] and Oliver and Pharr [2] proposed methods to extract the values of the Young's modulus of materials from the unloading part of indentation load–displacement curves. Based on three-dimensional finite element simulations, a set of equations for reverse analysis of indentation experiments was proposed by Giannakopoulos and Suresh [3], while Cheng and Cheng [4, 5] derived a set of dimensionless functions to relate the characteristics of the indentation load–displacement curve to the elasto-plastic properties of the material. Empirical methods to determine the Young's modulus and strain-hardening exponent from the unloading curve were presented by Zeng and Chiu [6] and Zeng and Shen [7]. Dao *et al* [8] proposed a new set of dimensionless functions, and forward and reverse analysis schemes based on extensive finite element simulations. Bucaille *et al* [9] and Chollacoop *et al* [10] subsequently extended the method proposed by Dao *et al* [8] for forward and reverse analyses based on dual sharp indenters. It was demonstrated by Swaddiwudhipong *et al* [11] that the latter is imperative for unique recovery of the three elasto-plastic material properties.

Owing to large geometric and material nonlinearities as well as complex contact problem at the indentation interface, closed form solutions are not readily available. At present, the most practical approach to the interpretation of the indentation load–displacement curve is a semi-analytical approach, whereby the forms of the governing relationships between the characteristics of the load–displacement curve and the elasto-plastic material properties are derived analytically and the underlying relationships calibrated numerically. The accuracy of such an approach is highly dependent on the precision of the curve or surface fitting procedure, as well as the robustness of the reverse analysis algorithm. A common practice is to express the characteristics of the indentation load–displacement curve as some functions of the elasto-plastic material properties and either the inverse or the point of intersection of several functions is established. Owing to the complexity of the functions a trial and error procedure is normally necessary, and consequently additional error could be introduced.

An artificial neural network approach has been successfully used to interpret indentation results. Huber *et al* [12, 13] presented artificial neural network models to determine the constitutive properties of thin films on a substrate based on the depth–load trajectory of spherical indentation. Their models enabled the material properties of both the thin film and the substrate to be identified from a single indentation load–displacement curve. More recently, Huber and Tyulyukovskiy [14] presented a sophisticated artificial neural network model to solve the inverse problem of determining the viscoplastic material properties from indentation load–displacement response subject to multiple creep processes.

In this study, an artificial neural network (ANN) model is constructed for material characterization based on simulated load–displacement response for dual sharp indenters. The artificial neural network is a robust tool to perform multi-dimensional function approximation. The artificial neural network approach circumvented the need to identify the form of the function prior to the establishment of the multi-dimensional fitting surfaces. Extensive finite element analyses are carried out in order to investigate the response of elasto-plastic materials obeying power law strain-hardening during indentation, using two indenters of different geometries. The numerical data from finite element analyses are used for the training and verification of the ANN model. The proposed artificial neural network model is robust, and directly relates the characteristics of the indentation load–displacement curve to the elasto-plastic material properties without resorting to an iterative procedure.

2. Finite element simulation

Conical indenters with half-angles of 60.0˚ and 70.3˚ are modelled as rigid bodies in the finite element models. Large strain and large deformation finite element analyses were carried out using ABAQUS, a commercial software. Each finite element mesh adopted for the target material consists of 28 900 four-node, bilinear, axisymmetric, quadrilateral elements. The model has been tested, *a priori*, to ensure the convergence of the finite element results and the insensitivity to far-field effects. As the effect of friction is negligible for any indenters with half-angles larger than 60˚ [9], frictionless contact is assumed in the present finite element model.

Materials obeying power law strain-hardening with the uniaxial true stress–true strain relationship expressed in equations (1) were considered in this study.

$$\sigma = E\varepsilon \qquad \text{for } \sigma \leqslant Y, \tag{1a}$$

$$\sigma = R\varepsilon^{n} \qquad \text{for } \sigma \geqslant Y. \tag{1b}$$

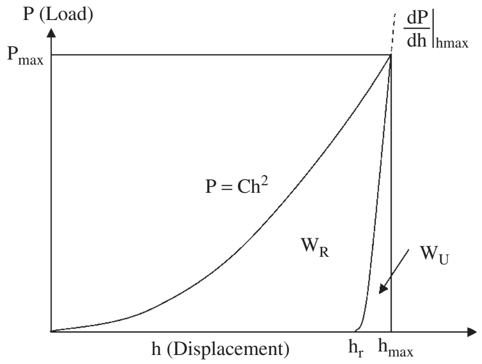

Figure 1. Typical representation of the load–displacement curve of an elasto-plastic material.

In equation (1), E is Young's modulus, Y the yield stress, R the strength coefficient and n the strain-hardening exponent.

Enforcing continuity at $\sigma = Y$ gives

$$R = Y\left(\frac{E}{Y}\right)^n. \tag{2}$$

If the elasticity effect of the indenter is significant and has to be considered in the analysis, the actual Young's modulus, E, of the targetted materials should be replaced by a reduced Young's modulus, E^*, expressed in equation (3) [3, 8, 10].

$$E^* = \left[\frac{1-\nu^2}{E} + \frac{1-\nu_i^2}{E_i}\right]^{-1}. \tag{3}$$

In equation (3), E_i and ν_i are the Young's modulus and Poisson ratio of the indenter, respectively. A constant Poisson ratio of 0.33 is used throughout this study.

3. Load–displacement curves

A typical indentation load–displacement curve of an elasto-plastic material such as Al6061 is shown in figure 1 [8, 10]. The loading part of an instrumented sharp indentation generally follows Kick's law which can be expressed as

$$P = Ch^2, \tag{4}$$

where P is the indentation load, h the penetration depth measured from the surface and C a constant curvature. The projected contact area for ideally sharp indenters with a linear relationship between the penetration depth and the contact radius can be expressed as

$$A = kh^2, \tag{5}$$

where k is constant for a particular material and indenter geometry.

Dividing equations (4) by (5) leads to

$$p_{\mathrm{ave}} = \frac{P}{A} = \frac{C}{k} = \text{constant}. \tag{6}$$

Based on the relationship derived by Luk *et al* [15],

$$\frac{p_{\mathrm{ave}}}{Y} = f\left(\frac{E^*}{Y}, n\right). \tag{7}$$

In view of equations (6) and (7), the following relationship between C and the three material parameters (E^*, Y, n) can be established.

$$\frac{C}{Y} = f_{1,\theta}\left(\frac{E^*}{Y}, n\right), \tag{8}$$

where θ is the half-angle of the indenter. Equation (8) is consistent with the expression derived by Cheng and Cheng [4] using dimensional analysis. The latter also showed that

$$\frac{W_{\mathrm{T}} - W_{\mathrm{U}}}{W_{\mathrm{T}}} = \prod_{\omega}\left(\frac{Y}{E}, \nu, \theta\right), \tag{9}$$

where W_{T} is the area under the loading curve and W_{U} the area under the unloading curve.

Denoting $(W_{\mathrm{T}} - W_{\mathrm{U}})$ by W_{R}, for a particular value of Poisson ratio and half-angle of the indenter, equation (9) becomes

$$\frac{W_{\mathrm{R}}}{W_{\mathrm{T}}} = f_{2,\theta}\left(\frac{E^*}{Y}, n\right). \tag{10}$$

4. Artificial neural network model

By substituting the values of $\theta = 60.0^\circ$ and 70.3°, equations (8) and (10) yield, respectively

$$\left.\frac{C}{Y}\right|_{60.0^\circ} = f_{1,60.0^\circ}\left(\frac{E^*}{Y}, n\right), \tag{11}$$

$$\left.\frac{C}{Y}\right|_{70.3^\circ} = f_{1,70.3^\circ}\left(\frac{E^*}{Y}, n\right), \tag{12}$$

$$\left.\frac{W_{\mathrm{R}}}{W_{\mathrm{T}}}\right|_{60.0^\circ} = f_{2,60.0^\circ}\left(\frac{E^*}{Y}, n\right), \tag{13}$$

$$\left.\frac{W_{\mathrm{R}}}{W_{\mathrm{T}}}\right|_{70.3^\circ} = f_{2,70.3^\circ}\left(\frac{E^*}{Y}, n\right). \tag{14}$$

Dividing equations (11) by (12) leads to equation (15).

$$\frac{C_{60.0^\circ}}{C_{70.3^\circ}} = \frac{f_{1,60.0^\circ}(E^*/Y, n)}{f_{1,70.3^\circ}(E^*/Y, n)} = f_3\left(\frac{E^*}{Y}, n\right). \tag{15}$$

The solution to the problem is represented by the point of intersection between the surfaces defined by equations (13)–(15). It has been shown earlier by Swaddiwudhipong *et al* [11] and Tho *et al* [16] that the reverse analysis based on dual sharp indenters leads to a unique solution of E^*/Y and n, and hence there exists only one point of intersection among the surfaces defined by equations (13)–(15). Therefore, there exists a one-to-one mapping of $(C_{60.0^\circ})/(C_{70.3^\circ})$, $(W_{\mathrm{R}}/W_{\mathrm{T}})_{60.0^\circ}$ and $(W_{\mathrm{R}}/W_{\mathrm{T}})_{70.3^\circ}$ to E^*/Y and n.

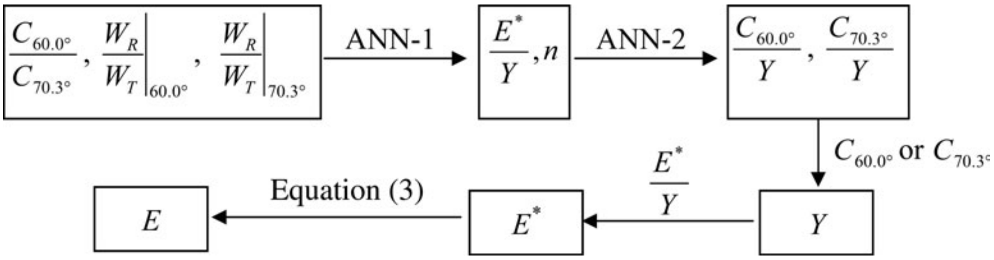

Figure 2. Flowchart illustrating the solution procedure.

Two artificial neural networks, denoted as ANN-1 and ANN-2, are constructed for the reverse analysis of instrumented indentation results. ANN-1 is constructed to map $(C_{60.0^\circ})/(C_{70.3^\circ})$, $(W_R/W_T)_{60.0^\circ}$ and $(W_R/W_T)_{70.3^\circ}$ to E^*/Y and n, while the mapping of E^*/Y and n to $(C_{60.0^\circ}/Y)$ and $(C_{70.3^\circ}/Y)$ is handled by ANN-2. Once ANN-1 and ANN-2 are constructed, the reverse analysis process is straightforward. From the indentation load–displacement curves of both indenters, the quantities $C_{60.0^\circ}$, $C_{70.3^\circ}$, $(W_R/W_T)_{60.0^\circ}$ and $(W_R/W_T)_{70.3^\circ}$ can be determined. By providing the values of these quantities to ANN-1, the ratio of E^*/Y and n can be determined and these results are then substituted into ANN-2 to obtain $(C_{60.0^\circ}/Y)$ and $(C_{70.3^\circ}/Y)$. Since $C_{60.0^\circ}$ and $C_{70.3^\circ}$ are known, Y can be calculated from either $(C_{60.0^\circ}/Y)$ or $(C_{70.3^\circ}/Y)$ and hence the results can be self-verified. Consequently, E^* can be evaluated from the ratio of E^*/Y established earlier. The actual value of Young's modulus, E, can then be obtained from equation (3). The solution procedure is summarized in the flowchart shown in figure 2.

Back-propagation multilayer feedforward ANNs (ANN-1 and ANN-2) were created using the Neural Network Toolbox in the Matlab 6.5 package. Both ANN-1 and ANN-2 comprise an input layer, a hidden layer and an output layer. The numbers of neurons in the input and output layers of the ANNs are identical to the numbers of input and output parameters, respectively. However, the number of neurons in the hidden layer of the neural network is calibrated during the training and validation process. The tangent sigmoid transfer function is used in the hidden layer while the linear transfer function is assigned to the output layer.

The ANNs are trained by introducing a set of examples (pairs of inputs and the corresponding outputs) of proper network behaviour to the ANNs. As the inputs are applied to the network, the network outputs are compared to the target outputs. During training, the learning rule is used to iteratively adjust the weights and biases of the network, in order to move the network outputs closer to the target values by minimizing the network performance indicator. The Levenberg–Marquardt training algorithm, which has a higher rate of convergence, is used for the training of both ANN-1 and ANN-2.

The data for training and validation of ANN-1 and ANN-2 were obtained numerically through 500 large strain, large deformation finite element analyses encompassing a domain of E^*/Y from 10 to 1000 and n varying from 0.0 to 0.6 for each of the conical indenters. Out of the 500 sets of input and output data, 400 sets were randomly assigned as training data while the remaining 100 sets were used for validation purposes. The mean square error (MSE) of the network outputs and the target values is used as the network performance indicator. In ANN-1, the values of output 1 (i.e. E^*/Y) vary from 10 to 1000 while those of output 2 (i.e. n) range from 0 to 0.6. In order to achieve weightings of the same order of magnitude for the contributions from the two outputs to the performance indicators, a scaled-down parametric value, $E^*/1000Y$, is adopted in ANN operations. ANN-1 and ANN-2 are trained using the training data sets and tested against the validation data sets.

Table 1. Characteristics of ANN-1 and ANN-2.

	Range of outputs	Number of neurons in the hidden layer	Mean square error	
			Training	Validation
ANN-1	0–1	30	1.398E−05	4.609E−05
ANN-2	10–610	24	4.555E−02	5.215E−02

The number of neurons in the hidden layer of the neural network has serious implications for the performance of the ANN. If too few neurons are used in the hidden layer, the ANN does not possess a sufficient degree of freedom to approximate the function relating the inputs and the outputs. On the other hand, if too many neurons are used in the hidden layer, over-fitting can occur. In such a situation, the trained ANN is able to predict the training data almost exactly but performs poorly with new sets of data. The determination of the number of neurons in the hidden layer is an iterative process. During the training process, the number of neurons in the hidden layer is increased slowly while the evolution of the training MSE and the validation MSE are tracked. Initially, both the training MSE and validation MSE decrease with increasing number of neurons in the hidden layer. However, after a certain threshold value of the number of neurons in the hidden layer is reached, the validation MSE will increase while the training MSE will continue to decrease due to the over-fitting phenomena. By identifying the turning point of the validation MSE, a good estimate of the optimal number of neurons in the hidden layer can be obtained. The characteristics of ANN-1 and ANN-2 are summarized in table 1.

5. Results and discussion

Finite element analyses were carried out to simulate indentation experiments on Al6061, Al7075, steel and iron. The typical elasto-plastic material properties of these materials [8, 9, 15] are used as inputs to the finite element model. The finite element results are summarized in table 2. It should be noted that these sets of finite element results were not used in the training and validation process described in section 4.

The solution procedure described in the previous section is then applied using the finite element results depicted in table 2 as inputs. The material properties predicted by the artificial neural network model are shown in table 3, together with the actual material properties. It can be observed from table 3 that the proposed artificial neural network model predicted the elasto-plastic material properties reasonably accurately. The relatively large percentage difference between the actual value of n and the predicted value of n is exaggerated to certain extent by the small value of n.

By training and validating ANN-1 and ANN-2 with the data sets from indenters of different geometries, the proposed artificial neural network model can be used to perform reverse analysis based on the results of other indenter geometries. Furthermore, the proposed artificial neural network model can be easily extended to perform a reverse analysis based on the results obtained from finite element simulations of multiple indenter geometries. The accuracy of the model is expected to improve significantly as results from more indenters are considered in the operations.

6. Conclusion

The artificial neural network is a robust tool to perform multi-dimensional surface fitting. Artificial neural networks enable the direct mapping of the characteristics of the indentation

Table 2. Summary of finite element results for Al6061, Al7075, steel and iron.

Material	Conical indenter with half-angle of 60.0° $C_{60.0^\circ}$ (GPa)	$C_{70.3^\circ}$ (GPa)	Conical indenter with half-angle of 70.3° $(W_R/W_T)_{60.0^\circ}$	$(W_R/W_T)_{70.3^\circ}$
Al6061	10.740	27.200	0.952	0.921
Al7075	20.362	46.555	0.903	0.853
Steel	23.907	59.272	0.960	0.937
Iron	24.598	55.513	0.949	0.925

Table 3. Prediction from artificial neural network model.

	Al6061	Al7075	Steel	Iron
E^* (GPa)				
Actual	72.4	73.4	194.3	170.8
Predicted	72.7	73.1	195.6	170.0
Deviation (%)	0.5	0.4	0.7	0.5
E (GPa)				
Actual	69.0	70.1	210.0	180.0
Predicted	69.3	69.8	211.8	179.0
Deviation (%)	0.5	0.4	0.8	0.6
Y (MPa)				
Actual	275.0	500.0	500.0	300.0
Predicted	276.3	508.3	489.6	297.9
Deviation (%)	0.5	1.6	2.1	0.7
n				
Actual	0.050	0.122	0.100	0.250
Predicted	0.049	0.117	0.106	0.253
Deviation (%)	2.3	4.5	5.6	1.2

load–displacement curve to the elasto-plastic material properties. The proposed artificial neural network model can accurately predict the elasto-plastic properties of the materials based on the simulated load–displacement curves of dual conical indenters with different half-angles. The proposed ANN model can also be extended for reverse analysis based on the results obtained from other indenter geometries.

Acknowledgment

The authors gratefully acknowledge Ooi Nick Sern, Brandon from the National University of Singapore for his assistance in the preparation and training of the artificial neural network model.

References

[1] Doerner M F and Nix W D 1986 A method for interpreting the data from depth-sensing indentation instruments *J. Mater. Res.* **1** 601–9

[2] Oliver W C and Pharr G M 1992 An improved technique for determining hardness and elastic modulus using load and displacement sensing indentation experiments *J. Mater. Res.* **7** 1564–83

[3] Giannakopoulos A E and Suresh S 1999 Determination of elastoplastic properties by instrumented sharp indentation *Scr. Mater.* **40** 1191–8

[4] Cheng Y T and Cheng C M 1998 Scaling approach to conical indentation in elastic–plastic solids with work hardening *J. Appl. Phys.* **84** 1284–91

[5] Cheng Y T and Cheng C M 1999 Scaling relationships in conical indentation of elastic–perfectly plastic solids *Int. J. Solids Struc.* **36** 1231–43

[6] Zeng K and Chiu C H 2001 An analysis of load–penetration curves from instrumented indentation *Acta Mater.* **49** 3539–51

[7] Zeng K and Shen L 2002 A new analysis of nanoindentation load–displacement curves *Phil. Mag.* A **82** 2223–9

[8] Dao M, Chollacoop N, Van Vliet K J, Venkatesh T A and Suresh S 2001 Computational modelling of the forward and reverse problems in instrumented sharp indentation *Acta Mater*. **49** 3899–918

[9] Bucaille J L, Stauss S, Felder E and Michler J 2003 Determination of plastic properties of metals by instrumented indentation using different sharp indenters *Acta Mater.* **51** 1663–78

[10] Chollacoop N, Dao M and Suresh S 2003 Depth-sensing instrumented indentation with dual sharp indenters *Acta Mater*. **51** 3713–29

[11] Swaddiwudhipong S, Tho K K, Liu Z S and Zeng K 2004 Material characterization based on dual indenters *Int. J. Solids Struc.* at press

[12] Huber N, Tsagrakis I and Tsakmakis Ch 2000 Determination of constitutive properties of think metallic films on substrates by spherical indentation using neural networks *Int. J. Solids Struc.* **37** 6499–516

[13] Huber N, Nix W D and Gao H 2002 Identification of elastic–plastic material parameters from pyramidal indentation of thin films *Proc. R. Soc.* A **458** 1593–620

[14] Huber N and Tyulyukovskiy E 2004 A new loading history for identification of viscoplastic properties by spherical indentation *J. Mater. Res.* **19** 101–13

[15] Luk V K, Forrestal M J and Amos D E 1991 Dynamic spherical cavity expansion of strain-hardening materials *J. Appl. Mech.* **58** 1–6

[16] Tho K K, Swaddiwudhipong S, Liu Z S, Zeng K and Hua J 2004 Uniqueness of reverse analysis from conical indentation tests *J. Mater. Res.* at press